Oligophenylenevinylene Phane Dimers: Probing the Effect of Contact Site on the Optical Properties of Bichromophoric Pairs

Shujun Wang,[†] **Guillermo C. Bazan,***,[†] **Sergei Tretiak,**[‡] **and Shaul Mukamel***,[‡]

Contribution from the Department of Chemistry, University of California,
Santa Barbara, California 93106, and the Department of Chemistry and Rochester Theory Center for
Optical Science and Engineering, University of Rochester, Rochester, New York 14627

Abstract: Paracyclophane derivatives have been prepared that may be considered models of bichromophoric contacts in the solid. The optical properties of these compounds give insight into how bringing two chromophores into close proximity affects the photophysics of the pair. Thus, reaction of 4,7,12,15-tetrabromo[2.2]-paracyclophane (4,7,12,15-**Br₄Pc**) with excess 4-*tert*-butylstyrene using Pd(OAc)₂ under phase transfer conditions affords 4,7,12,15-tetra(4-*tert*-butylstyryl)[2.2]paracyclophane (**3R_D**). The connectivity of **3R_D** models a contact between two distyrylbenzene molecules across the central ring. Reaction of 4,7,12,15-**Br₄Pc** with 4-(4-*tert*-butylstyryl)styrene (**TBSS**) under similar conditions gives 4,7,12,15-tetra(4-(4′-*tert*-butylstyryl)styryl)[2.2]-paracyclophane (**5R_D**). In **5R_D** two oligophenylenevinylene units containing five phenyl rings are connected via their central ring. Similar reaction protocols gave 2,5-dimethyl-1,4-di(4-*tert*-butylstyryl)benzene (**3R**) and 2,5-dimethyl-1,4-bis[4-(4′-*tert*-butylstyryl)styryl]benzene (**5R**). Molecules **3R** and **5R** serve to give the optical properties of the monomeric units. Comparison against the properties of **3R** and **5R** shows that the absorption and emission data of **3R_D** and **5R_D** are consistent with considerable delocalization between the two subunits across the paracyclophane bridge. The observed trends in the optical properties of these compounds are analyzed using collective electronic oscillators (CEO) representing the changes induced in the electronic density matrix upon optical excitation. Comparison of the CEO of the paracyclophane dimers with the corresponding monomers using two-dimensional plots provides an efficient method for tracing the origin of the various optical and electronic transitions by identifying the underlying changes in charge densities and bond orders. The electronic description of **3R_D** and **5R_D**, in which the interchromophore contact is across the central ring, is considerably different from the description of paracyclophane dimers of similar chromophores that are connected via the terminal ring. Essentially no delocalization is observed for the "termini" dimers.

Introduction

Chromophore−chromophore interactions are a critical consideration for designing technologically relevant optoelectronic materials. The charge transport properties of organic materials depend on the relative orientation and distance between individual molecules in the solid. Proper molecular alignment over long distances allows for better charge transport and lower operating voltages in organic transistors.[1] For polymer-based light-emitting diodes, ordered regions lead to excimer formation and a reduced electroluminescence quantum yield.[2,3] Because multiple environments are often present in solid samples, it is difficult to ascertain to a high level of precision how the environment surrounding an individual chromophore affects properties of interest.[4] The study of polychromophores in dilute solution is complicated by intrachain contacts that lead to energy transfer or excimer formation.[5] Well-defined molecules that are representative of chromophore aggregates in the solid and that can be studied in the absence of interactions with other chromophores give insight into the effect of through-space delocalization on the photophysics of the aggregate.

The importance of the optical response of chromophore aggregates extends into various branches of chemical science. Significant attention has been devoted to studies of clusters in supersonic beams,[6,7] J-aggregates of cyanine dyes,[8] supramolecular structures,[9] and biological complexes (photosynthetic antennae and reaction centers).[10] It is possible to treat aggregates as giant molecules and employ methods of quantum

† University of California.
‡ University of Rochester.
(1) (a) Servet, B.; Horowitz, G.; Ries, S.; Lagorsse, O.; Alnot. P.; Yassar, A.; Deloffre, F.; Srivastava P.; Hajlaoui, R.; Lang, P.; Garnier, F. *Chem. Mater.* **1994**, *6*, 1809. (b) Dodalabalapur, A.; Torsi, L.; Katz, H. E. *Science* **1995**, *268*, 270.
(2) (a) Conwell, E. *Trends Polym. Sci.* **1997**, *5*, 218. (b) Cornil, J.; dos Santos, D. A.; Crispin, X.; Silbey, R.; Bredas, J. L. *J. Am. Chem. Soc.* **1998**, *120*, 1289.
(3) (a) Lee, C. H.; Yu, G.; Moses, D.; Heeger, A. J. *Synth. Met.* **1995**, *69* (1−3), 429. (b) Gettinger, C. L.; Heeger, A. J.; Drake, J. M.; Pine, D. J. J. *Chem. Phys.* **1994**, *101*, 1673. (c) Kohler, A.; Gruner, J.; Friend, R. H.; Mullen, K.; Scherf, U. *Chem. Phys. Lett.* **1995**, *243*, 456.

(4) (a) Guillet, J. *Polymer Photophysics and Photochemistry*; Cambridge University Press: Cambridge, U.K., 1985. (b) *Photophysics of Polymers*; Hoyle, C. E., Torkelson, J. M., Eds.; ACS Symp. Ser. 358; American Chemical Society: Washington, DC, 1987. (c) Winnik, F. M. *Chem. Rev.* **1993**, *93*, 587.
(5) Miao, Y.-J.; Herkstroeter, W. G.; Sun, B. J.; Wong-Foy, A. G.; Bazan, G. C. *J. Am. Chem. Soc.* **1995**, *117*, 11407.
(6) (a) Easter, D. C.; Whetten, R. L.; Wessel, J. E. *J. Chem. Phys.* **1991**, *94*, 3347. (b) Easter, D. C.; Khoury, J. T.; Whetten, R. L. *J. Chem. Phys.* **1992**, *97*, 1681. (c) Easter, D. C.; Baronavski, A. P.; Whetten, R. L. *J. Chem. Phys.* **1993**, *99*, 4942.
(7) (a) Syage, J. A.; Wessel, J. E. *J. Chem. Phys.* **1988**, *89*, 5962. (b) Wessel, J. E.; Syage, J. A. *J. Phys. Chem.* **1990**, *94*, 737.
(8) Mukamel, S., Chemla, D. S., Eds.; Special Issue, Confined Excitations in Molecular and Semiconductor Nanostructures. *Chem. Phys.* **1996**, *210*.

chemistry to calculate their electronic structure. These approaches are limited to small aggregates.[11,12] An important goal of computational chemistry is to trace the electronic states and spectra of aggregates to those of their basic building blocks, the monomers. By doing so it should become possible to get a better microscopic insight into the nature of their electronic excitations and to predict qualitative features of complex large systems using simple, readily available information. Predicting qualitative features of complex multicomponent ensembles from readily available information should then become possible on isolated molecules.

In an effort to achieve some of the goals stated above, we recently reported a series of molecules whose structures mimic stilbene and distyrylbenzene dimers.[13] Examples include molecules **1a**, **1b**, **2a**, and **2b** shown below (in these drawings ring deformations due to strain are not shown).

1a   **1b**   **2a**   **2b**
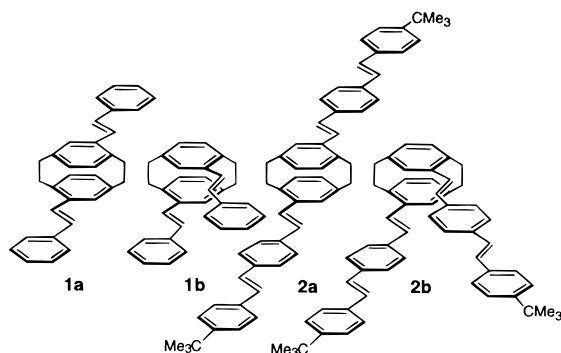
The rigid paracyclophane core (**Pc**)[14] was chosen as a center of convergence since it holds two arene rings in close proximity and because it has proven valuable in the study of ring strain and $\pi-\pi$ delocalization in organic molecules.[15] Molecules of this type have been used previously to imitate interchromophore contacts in the solid state and excimer properties.[16] Comparison

side view   (**Pc**)   top view
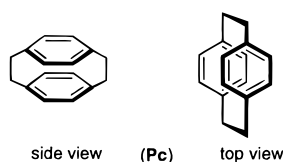
of the optical data from the paracyclophane dimers against data from monomeric units provides information on the effect of bringing together the two molecules into close proximity. For

Scheme 1

a, for R = H, Ph   **b**, for R* = H,4-^{t}Bu- Ph

example, the optical properties of **1a** or **1b** (stilbene dimers) can be compared against those of stilbene. Our focus on stilbene and distyrylbenzene fragments stems from the importance of stilbene in delineating photoisomerization processes in organic molecules[17] and the widespread use of poly(*p*-phenylenevinylene) (PPV) derivatives in new display technologies.[18]

A combination of spectroscopic and computational efforts produced the qualitative energy diagram shown in Scheme 1 to explain the photophysics of **1a**, **1b**, **2a**, and **2b**.[19] We determined that in all cases the most significant absorption is attributed to the "monomer" chromophore, i.e., stilbene in the case of **1a**. There is a second "phane" excited state to consider which contains the paracyclophane core with through-space ($\pi-\pi$) delocalization.[20] Emission from this state is broad and featureless and similar to that which characterizes excimers.

Two situations may be encountered with regard to photoluminescence. For smaller chromophores such as stilbene, the energy of the localized excitation is higher than that of the state containing the paracyclophane core (**a**, Scheme 1). Energy

(9) (a) Berberan-Santos, M. N.; Canceill, J.; Brochon, J.-C.; Jullien, L.; Lehn, J.-M.; Pouget, J.; Tauc, P.; Valeur, B. *J. Am. Chem. Soc.* **1992**, *114*, 6227. (b) Berberan-Santos, M. N.; Pouget, J.; Tauc, P.; Valeur, B.; Canceill, J.; Jullien, L.; Lehn, J.-M. *J. Phys. Chem.* **1993**, *97*, 11376. (c) Berberan-Santos, M. N.; Canceill, J.; Gratton, E.; Jullien, L.; Lehn, J.-M.; So, J.; Sutin, J.; Valeur, B. *J. Phys. Chem.* **1996**, *100*, 15.

(10) Special Issue on Light-Harvesting Physics Workshop. *J. Phys. Chem. B* **1997**, *101*. Sundström, V.; van Grondelle, R. In *Anoxygenic Photosynthetic Bacteria*; Blankenship, R. E., Madiga, M. T., Baner, C. E., Eds.; Kluwer Academic: Dordrecht, 1995; p 349.

(11) (a) Scholes, G. D.; Ghiggino, K. P.; Oliver, A. M.; Paddon-Row, M. N. *J. Am. Chem. Soc.* **1993**, *115*, 4345. (b) Clayton, A. H. A.; Scholes, G. D.; Ghiggino, K. P.; Paddon-Row,: M. N. *J. Phys. Chem.* **1996**, *100*, 10912.
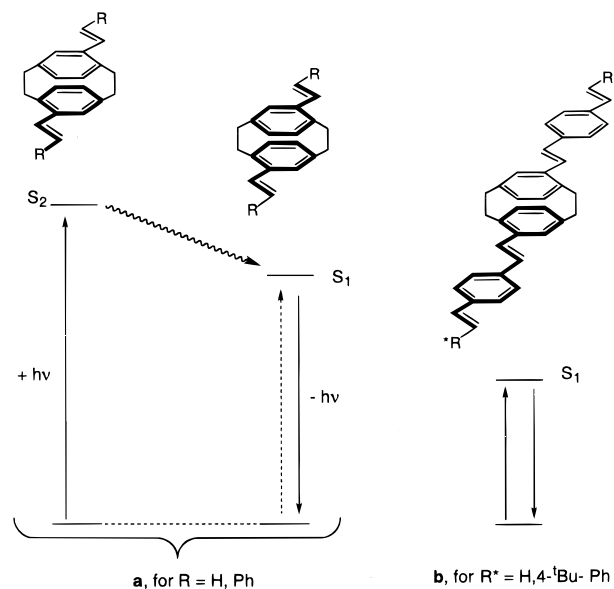
(12) (a) Hobra, P.; Selzle, H. L.; Schlag, E. W. *J. Am. Chem. Soc.* **1994**, *116*, 3500. (b) Börsen, K. O.; Lin, S. H.; Selzle, H. L.; Schlag, E. W. *J. Chem. Phys.* **1989**, *90*, 1299. (c) Cársky, P.; Selzle, H. L.; Schlag, E. W. *Chem Phys.* **1988**, *125*, 166.

(13) Oldham, W. J., Jr.; Miao, Y.-J.; Lachicotte, R. J.; Bazan, G. C. *J. Am. Chem. Soc.* **1998**, *120*, 419.

(14) Cram, D. J.; Bauer, R. H. *J. Am. Chem. Soc.* **1959**, *81*, 5971.

(15) Voegtle, F. *Cyclophane Chemistry*; J. Wiley & Sons: New York, 1993.

(16) Chromophores studied in this manner include the following. (a) Phenanthrenophane: Schweitzer, D.; Hausser, K. H.; Haenel, M. *Chem. Phys.* **1978**, *29*, 181. (b) Anthracenophane: Ishikawa, S.; Nakamura, J.; Iwata, S.; Sumitami, M.; Nagakura, S.; Sakata, Y.; Misumi, S. *Bull. Chem. Soc. Jpn.* **1979**, *52*, 1346. (c) Fluorenophane: Haenel, M. W. *Tetrahedron Lett.* **1976**, *36*, 3121. (d) Colpa, J. P.; Hausser K. H.; Schweitzer, D. *Chem. Phys.* **1978**, *29*, 187. (d) Pyrenophane and several isomers of naphthalenophane: Haenel, M.; Staab, H. A. *Chem. Ber.* **1973**, *106*, 2203. Otsubo, T.; Mizogami, S.; Osaka, N.; Sakata, Y.; Misumi, S. *Bull. Chem. Soc. Jpn.* **1977**, *50*, 1858. For studies of cycloaddition reactions see: (e) Grieiving, H.; Hopf, H.; Jones, P. G.; Bubenitscheck, P.; Desvergne, J. P.; Bouas-Laurent, J. *J. Chem. Soc., Chem. Commun.* **1994**, 1075. (f) Okada, Y.; Ishii, F.; Akiyama, I.; Nishimura, J. *Chem. Lett.* **1992**, 1579. (g) Ferguson, J. *Chem. Rev.* **1986**, *86*, 957. (h) Grieiving, H.; Hopf, H.; Jones, P. G.; Bubenitscheck, P.; Desvergne, J. P.; Bouas-Laurent, *Liebigs. Ann.* **1995**, 1949. (i) Marquis, D.; Desvergne, J. P.; Bouas-Laurent, H. *J. Org. Chem.* **1995**, *60*, 7984.

(17) (a) Saltiel, J.; Sun, Y.-P. In *Photochromism, Molecules and Systems*; Dürr, H., Bouas-Laurent, H., Eds.; Elsevier: Amsterdam, 1990; pp 64−164. (c) For a review of the relevance of stilbene chemistry and photophysics to materials science see: Meier, H. *Angew. Chem., Int. Ed. Engl.* **1992**, *31*, 1399.

(18) Kraft, A.; Grimsdale, A. C.; Holmes, A. B. *Angew. Chem., Int. Ed. Engl.* **1998**, *37*, 402.

(19) Bazan, G. C.; Oldham, W. J., Jr.; Lachicotte, R. J.; Tretiak, S.; Chernyak, V.; Mukamel. S. *J. Am. Chem. Soc.* **1998**, *120*, 9188.

(20) (a) Canuto, S.; Zerner, M. C. *J. Am. Chem. Soc.* **1990**, *112*, 2114. (b) Iwata, S.; Fuke, K.; Sasaki, M.; Nagakura, S.; Otsubo, T.; Misumi, S. *J. Mol. Spectrosc.* **1973**, *46*, 1.

migration[21] after photon absorption transfers the excitation from the localized "monomer", and emission takes place from the "phane" state. The latter carries a very weak oscillator strength to the ground state. Population of the "phane" state via energy transfer thus results in a relatively long-lived excited state.

The second situation occurs when the energy of the "monomer" state is lower than that of the corresponding "phane" state (**b**, Scheme 1). This is the case for distyrylbenzene (**2a,b**). Under these circumstances there is no driving force for energy migration and the excitation remains localized at the initially generated state. Except for the spectral shift due to the **Pc** moiety, there is therefore negligible difference between the spectra of the parent compounds and the dimers **2a,b**.

In this contribution we report on the synthesis, spectroscopy, and quantum chemical analysis of paracyclophane dimers that bring together oligophenylenevinylene chromophores into contact by way of the central ring. These molecules provide information on how the electronic structure of these model chromophores changes by making a contact across the central ring. We will refer to this interaction as "criss-cross" to differentiate it from the "terminal" contact probed by molecules **1a,b** and **2a,b**. These efforts are aimed at understanding the effect of contact regiochemistry on the photophysics of the pair. We will find that the localization and the type of excitation are quite different in the criss-cross dimers, relative to their termini counterparts.

Results and Discussion

Synthesis and Characterization. Bromination of **Pc** by use of liquid bromine and a catalytic amount of iodine gives equal amounts of the isomeric tetrabromides 4,7,12,15-tetrabromo-[2.2]paracyclophane (4,7,12,15-**Br₄Pc**) and 4,5,12,13-tetrabromo-[2.2]paracyclophane (4,5,12,13-**Br₄Pc**) in 90% yield.[22] Separation by repeated crystallization in acetone affords the desired 4,7,12,15-**Br₄Pc** in 40% yield.

4,5,12,13-**Br₄Pc**   4,7,12,15-**Br₄Pc**
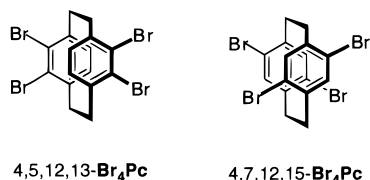
The stilbenoid arms are constructed by Heck reaction[23] under the phase transfer conditions reported by Jeffrey (excess K_2CO_3 and $BrNBu_4$ in DMF).[24] For example, reaction of an excess of 4-*tert*-butylstyrene with 4,7,12,15-**Br₄Pc** in the presence of Pd(OAc)₂ for 4 days affords the 4-fold coupled product 4,7,12,15-tetra(4-*tert*-butylstyryl)[2.2]paracyclophane (**3R_D** for the three-ring dimer) in 55% yield (eq 1). As the

(1)

3R_D
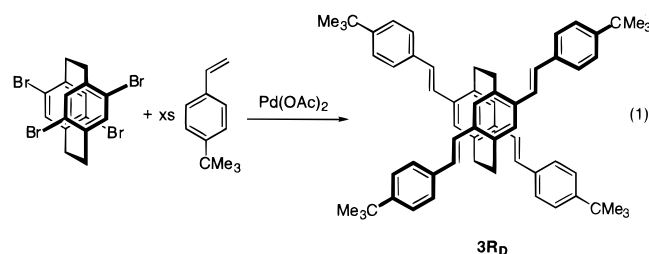
(21) Here we use the term "energy migration" but it could be argued that the term "internal conversion" is adequate as well.

(22) König, B.; Knieriem, B.; Meijere, A. *Chem. Ber.* **1993**, *126*, 1643.

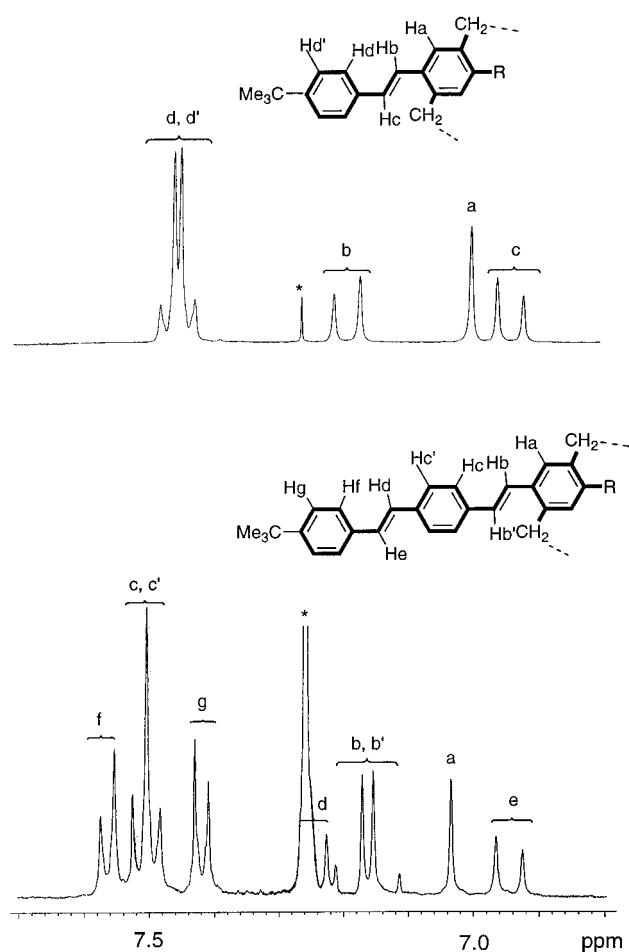(23) Heck, R. F. *Org. React.* **1982**, *27*, 345.

Figure 1. ¹H NMR spectra (CDCl₃, 400 MHz) in the aromatic and olefinic region for (a) **3R_D** and (b) **5R_D**. Inset shows the assignment of unique resonances. Solvent peak is denoted by an asterisk.

reaction progresses a gray precipitate forms and the solution becomes strongly fluorescent when illuminated. The composition of **3R_D** was confirmed by NMR spectroscopy and mass spectrometry. The ¹H NMR signals in the olefinic and aromatic regions are highly diagnostic (Figure 1).

A similar approach starting with 4-(4-*tert*-butylstyryl)styrene (**TBSS**) provides the analogue of **3R_D** with increased conjugation length. The requisite **TBSS** was obtained by the addition in small portions of NaH into a THF slurry of 4-vinylbenzylphosphonium chloride and 4-*tert*-butylbenzaldehyde, followed by stirring at room temperature for 24 h. The resulting cis and trans mixture of isomers (55% and 45%, respectively, by NMR) can be converted to exclusively the trans isomer by use of a catalytic amount of iodine in degassed benzene.

Attempts to react an excess of **TBSS** with 4,7,12,15-**Br₄Pc** in DMF using Pd(OAc)₂ invariably gave a mixture of coupling products in which the 4-fold coupled product was the minor component. These reactions do not reach completion even with prolonged reaction times and larger doses of catalyst. It appears that the 2-fold and 3-fold coupled intermediates precipitate out of solution because of their limited solubility in DMF. Improved yields are obtained using dimethylacetamide (DMA) under dilute conditions and 23 mol % of catalyst. Thus, reaction of **TBSS** with 4,7,12,15-**Br₄Pc** in DMA affords 4,7,12,15-tetra(4-(4′-*tert*-butylstyryl)styryl)[2.2]paracyclophane (**5R_D** for the five-ring dimer, in eq 2) in 18% yield as a slightly soluble yellow powder.

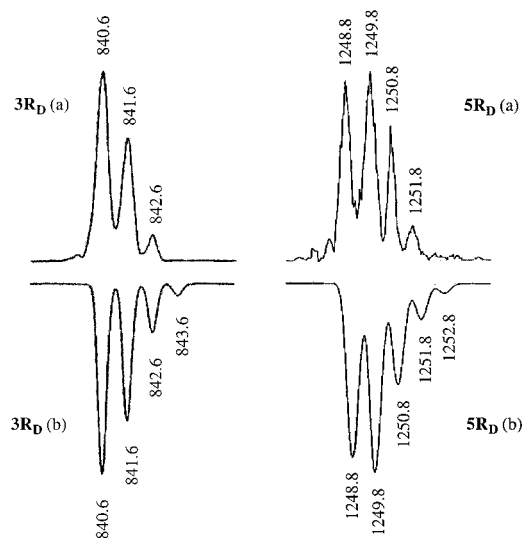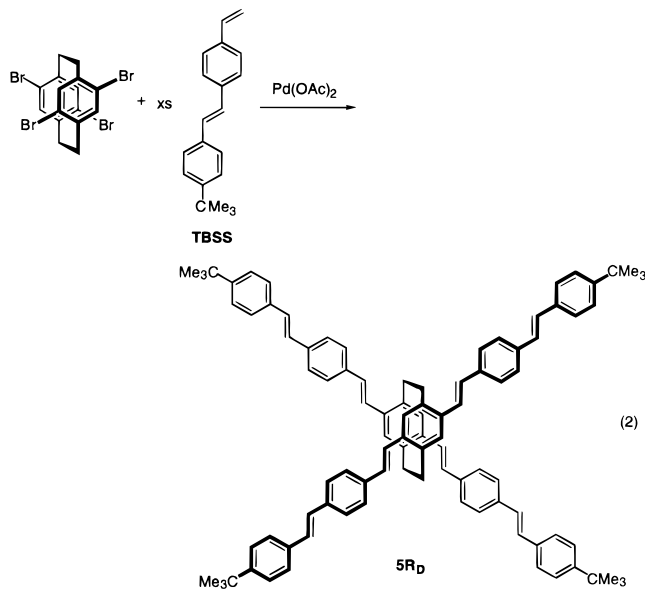(24) Jeffery, T. *Adv. Metal-Org. Chem.* **1996**, *5*, 153.

1292 *J. Am. Chem. Soc., Vol. 122, No. 7, 2000*

Wang et al.

Figure 2. Mass spectrometry peak for compounds **3R$_D$**, and **5R$_D$**: (a) experimental data and (b) simulation.

Characterization by ^{1}H NMR (Figure 1), HPLC, and mass spectrometry (Figure 2) confirms the composition of **5R$_D$**.

Reaction of *tert*-butylstyrene or **TBSS** with 2,5-dibromo-*p*-xylene affords 2,5-dimethyl-1,4-di(4-*tert*-butylstyryl)benzene (**3R**) and 2,5-dimethyl-1,4-bis[4-(4′-*tert*-butylstyryl)styryl]ben-zene (**5R**), respectively. **3R** is white and freely soluble in organic solvents. In comparison, **5R** is a yellow crystalline material which exhibits very poor solubility. Compounds **3R** and **5R** will serve as the "monomeric" units of **3R$_D$** and **5R$_D$** and will be useful for providing a baseline measure of the optical properties of the isolated chromophores.

Calculational Studies. To understand the root cause for the differences in optical behavior of the dimer molecules **3R$_D$** and **5R$_D$** relative to their corresponding monomeric units **3R** and **5R** we need to build an accurate model for the photoexcitation processes. The collective electronic oscillator (CEO) approach[25−28] provides a new effective computational scheme for electronic
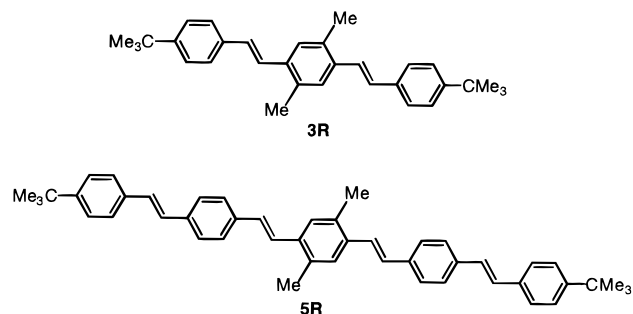
excitations of large molecules such as **3R$_D$** and **5R$_D$**. The numerical procedure for calculating electronic structure has been described in detail elsewhere.[13,19] The ZINDO code was applied first to generate the INDO/S Hamiltonian[29−32] using ground-state geometries obtained with the crystal X-ray diffraction data given in ref 13. We next calculated the Hartree−Fock ground-state density matrices[33,34] which are the input to the following CEO calculation. The CEO/DSMA procedure[13,19] was finally applied to compute the linear absorption spectra and the relevant transition density matrices which constitute the *electronic normal modes* ξ_ν. Each mode is a matrix representing the electronic transition between the ground state $|g\rangle$ and an electronically excited state $|\nu\rangle$. Its matrix elements are given by

$$(\xi_\nu)_{mn} = \langle \nu | c_m^+ c_n | g \rangle \qquad (3)$$

where $c_m^+ (c_m)$ are creation (annihilation) operators of an electron at the *m*-th atomic orbital, and $|g\rangle$ ($|\nu\rangle$) is the ground (excited) state many electron wave function. The modes can be obtained as eigenmodes of the linearized time-dependent Hartree−Fock (TDHF) equations of motion for the density matrix driven by the external field, totally avoiding the explicit calculation of many-electron eigenstates. The eigenfrequencies Ω_ν of these equations provide the optical transition frequencies.[13,19]

The frequency-dependent linear polarizability $\alpha(\omega)$ is then represented by

$$\alpha(\omega) = \sum_\nu \frac{f_\nu}{\Omega_\nu^2 - (\omega + i\Gamma)^2} \qquad (4)$$

where $f_\nu = 2\Omega_\nu [Tr(\mu\xi_\nu)]^2$ is the oscillator strength of the *g* to ν transition. Γ is the line width, and μ is the dipole moment operator. In all calculations we used the empirical line width $\Gamma = 0.2$ eV, and satisfactory convergence of the linear absorption was achieved using 10−15 effective electronic modes.

The electronic modes represent collective motions of electrons and holes and carry substantially less information than the many-electron eigenstates but more than required for calculating molecular polarizabilities and spectroscopic observables. The

(25) (a) Takahashi, A.; Mukamel, S. *J. Chem. Phys.* **1994**, *100*, 2366. (b) Mukamel, S.; Takahashi, A.; Wang, H. X.; Chen, G. *Science* **1994**, *266*, 251. (c) Chernyak, V.; Mukamel, S. *J. Chem. Phys.* **1996**, *104*, 444

(26) Mukamel, S.; Tretiak, S.; Wagersreiter, T.; Chernyak, V. *Science* **1997**, *277*, 781.

(27) (a) Tretiak, S.; Chernyak, V.; Mukamel, S. *Chem. Phys. lett.* **1996**, *259*, 55. (b) Tretiak, S.; Chernyak, V.; Mukamel, S. *J. Chem. Phys.* **1996**, *105*, 8914.

(28) Tretiak, S.; Chernyak, V.; Mukamel, S. *J. Am. Chem. Soc.* **1997**, *119*, 11408.

(29) Pople, J. A.; Segal, G. A. *J. Chem. Phys.* **1965**, *43*, S136.

(30) Pople, J. A.; Beveridge, D. L.; Dobosh, P. *J. Chem. Phys.* **1967**, *47*, 2026.

(31) Ridley, J.; Zerner, M. C. *Theor. Chim. Acta* **1973**, *32*, 111.

(32) Zerner, M. C.; Loew, G. H.; Kirchner, R. F.; Mueller-Westerhoff, U. T. *J. Am. Chem. Soc.* **1980**, *102*, 589.

(33) Mcweeny, R.; Sutcliffe, B. T. *Methods of Molecular Quantum Mechanics*; Academic Press: New York, 1976.

(34) Davidson, E. R. *Reduced Density Matrices in Quantum Chemistry*; Academic Press: New York, 1976.
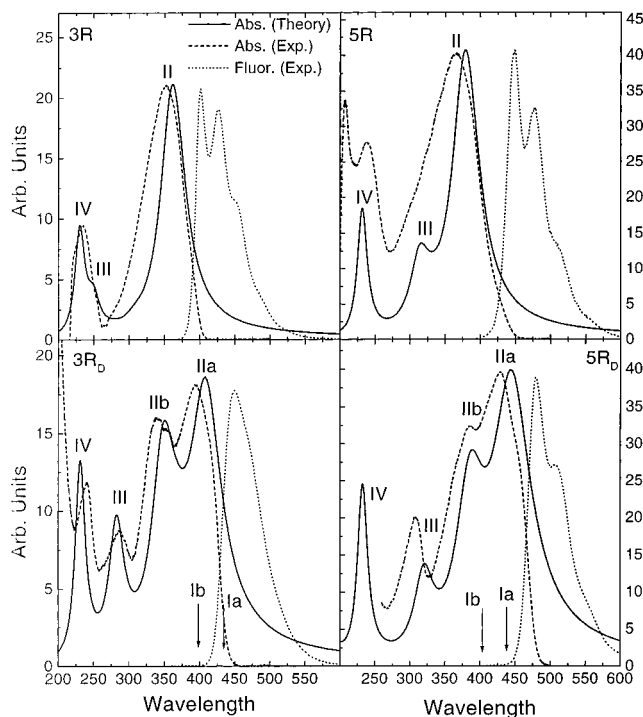
Figure 3. Calculated (solid lines) and experimental (dashed lines) absorption spectra and experimental (dotted lines) fluorescence spectra of **3R**, **3R_D**, **5R**, and **5R_D**. Emission spectra were measured by exciting at the absorption maxima.

diagonal elements $(\xi_\nu)_{nn}$ represent the net charge induced on the n-th atomic orbital by an external field, whereas $(\xi_\nu)_{mn}$ $m \neq n$ is the dynamical bond order representing the joint amplitude of finding an electron on orbital m and a hole on orbital n. Two-dimensional representation of electronic modes allows us to interpret and visualize electronic motions in terms of collective dynamics of the electronic density matrix.

Optical Properties. Figure 3 shows the experimental absorption and emission data for **3R**, **3R_D**, **5R**, and **5R_D** together with the corresponding calculated linear absorption spectra (solid lines). Table 1 summarizes the calculated frequencies. Overall, there is an excellent match between the experimental and calculated spectra. The long wavelength tail in the calculated spectra comes from the Lorentzian broadening assumed in the calculations.[35] Relative to distyrylbenzene, alkyl substitution on the center ring and the two end rings results in only a 162 cm^{-1} red shift at the absorption maximum of **3R**, probably because the methyl groups in the inner ring disfavor a coplanar arrangement with the two olefin side groups and cancel the alkyl substitution effect. The absorption spectrum of **3R_D** shows a split peak and a considerably red shifted absorption maximum (3028 cm^{-1}). The most prominent difference between the two is the split appearance of the absorption from **3R_D**. The vibronic structure is better defined in the emission of **3R** than in **3R_D**. The photoluminescence quantum yields for **3R** and **3R_D** are similar: 0.68 and 0.75 for **3R** and **3R_D**, respectively.

From Figure 3 we note that the line shape of **5R** is similar to that of **3R** and the absorption maximum is red shifted as expected. Interestingly, the absorption maximum for **5R_D**, appearing at 429 nm, is considerably red shifted from that of **5R** or even standard samples of PPV.[36] These observations

(35) A more rigorous modeling of the line profiles should include inhomogeneous (Gaussian) broadening, as well as vibronic structure, which go beyond the present analysis.

(36) Bazan, G. C.; Miao, Y.-J.; Renak, M. L.; Sun, B. J. *J. Am. Chem. Soc.* **1996**, *118*, 2618.

suggest considerable delocalization across the paracyclophane bridge. The fluorescence quantum yields of **5R** and **5R_D** are 0.56 and 0.54, respectively. The high fluorescence quantum yields of **3R**, **3R_D**, **5R**, and **5R_D** (compared with stilbene) suggest that these molecules attain a considerably more rigid and planar singlet excited state. For **3R**, **3R_D**, **5R**, and **5R_D**, the fluorescence excitation spectra match closely the absorption spectra.

Electronic Modes and Linear Absorption. We start our analysis from **3R** and **3R_D**. Following ref 19 the lowest strong absorption peak of **3R** is denoted as II. The other two features are denoted as III and IV (see Figure 3). To explore the origin of various peaks we examined the collective modes corresponding to these electronic excitations. Two-dimensional plots[19,26,28] of the matrices ξ_ν help establish a direct real-space connection between the optical response and the dynamics of charges upon optical excitation. The size of the matrix is equal to the number of carbon atoms in the molecule, labeled according to Figure 4a; the ordinate and abscissa represent an electron and a hole, respectively.

Panel 3R(II) in Figure 4b shows the electronic mode of peak II in **3R**. This mode is completely delocalized over the entire molecule with the strongest coherences (off-diagonal elements) in the double bonds of the vinylic groups. The following mode III of **3R** is localized on the phenyl−vinylene units with strongest coherences on the central arene ring. Finally, 3R(IV) is completely localized on the arene rings.

Before turning to the **3R_D** dimer spectra we recall a few properties of electronic modes in the absorption spectrum of **Pc**,[19] which is an important common unit of **3R_D** and **5R_D**. The absorption spectrum of **Pc** shows three electronic excitations. The lowest transition 1a is forbidden in linear absorption and shows up in the fluorescence. Higher frequency 1b is the first weak peak in absorption and, finally, high-frequency transition III dominates the absorption. All of these electronic modes are localized on the aromatic rings and show a strong electronic coherence (which is a signature of charge delocalization) between them.[37]

Panel 3R_D(Ia) of Figure 5 shows the lowest frequency electronic mode Ia of **3R_D**. This mode, which stems from the lowest transition in **Pc**, is essentially localized on the paracyclophane core and has a vanishing oscillator strength. The off-diagonal areas on central phenyls and neighboring vinylic groups represent the charge delocalization between monomers. The following mode 3R_D(Ib) corresponds to the next **Pc** mode and similarly has a weak oscillator strength. However, compared to **Pc** and the "termini collision" dimers, the 3R_D(Ia) and 3R_D(Ib) modes have significant delocalization on the vinylic groups adjacent to the central arene rings. In some sense this delocalization reflects the regiochemistry of the contact.

Mode 3R_D(IIa) originates from mode II of the monomer **3R** (diagonal blocks) and shows significant electronic coherences between chromophores (off-diagonal blocks). The structure of 3R_D(IIb) is similar to 3R_D(IIa) but it shows a different distribution of coherences. The strong coupling of the monomeric modes 3R(II) leads to a splitting of about 0.5 eV between modes IIa and IIb in the dimer. The 3R(II) modes appear in the absorption spectrum with large and comparable oscillator strength. Compared to "termini collision" dimers,[19] type II modes show much stronger interaction between chromophores. To explain this we recall that monomeric mode II has as the largest coherences the central phenyl and neighboring vinylic

(37) The CEO analysis of [2,2] paracyclophane, **Pc**, which is the central piece of all dimers studied, is given in ref 13.

Table 1. Computed Frequencies (in eV and cm^{-1})

	Pc	**3R**	**3R$_D$**	**5R**	**5R$_D$**
Ia	3.95 (31857)		2.87 (23147)		2.85 (22985)
Ib	4.77 (38470)		3.27 (26373)		3.17 (25566)
IIa		3.50 (28227)	3.03 (24437)	3.27 (26373)	2.78 (22421)
IIb			3.56 (28711)		3.21 (25889)
III		4.96 (40002)	4.39 (35405)	3.95 (31857)	3.87 (31212)
IV	5.5 (44358)	5.38 (43390)	5.37 (43309)	5.35 (43148)	5.33 (42986)

groups, i.e., the electron−hole pair "spends time" in the middle of the molecule. The interaction between excitons through the center ("central collision" dimers) is much stronger than that through the ends ("termini collision" dimers) of monomers.

The high-frequency modes 3R$_D$(III) and 3R$_D$(IV) arise from 3R(III) and 3R(IV) monomeric modes, respectively. They manifest themselves with strong intensities in the absorption spectra, show the same localization properties and, again, have significant optical coherences between the monomers. We thus conclude that the electronic excitations of the dimer **3R$_D$** originate from the excitations of its **Pc** and **3R** units with strong interaction between monomers compared to the "termini collision" dimers.

We next turn to **5R** and **5R$_D$**. The second row in Figure 4b shows the dominant electronic modes of **5R**. They have basically the same properties as the corresponding modes of the shorter molecule **3R**. The delocalized mode II is red-shifted. Transition III exhibits delocalization to the two phenyl−vinylene units at the molecular ends and is therefore red-shifted as well compared to 3R(III). In contrast, the 5R(IV) mode is completely localized at the phenyls and does not shift.

As shown in Figure 5, the electronic modes of **5R$_D$** originate from the correspondent excitations of **Pc** and **5R** units and show a strong interaction between the monomers fragments similar to that observed in **3R$_D$**. The principal difference between **3R$_D$** and **5R$_D$** is the frequency position of Ia and Ib peaks. In molecule **3R$_D$** transition Ia corresponds to the lowest frequency transition. In longer dimers **5R$_D$**, the state IIa is significantly red-shifted since it is delocalized, whereas the state Ia does not shift and, consequently, the state IIa is the lowest energy state.

An indirect confirmation of our predicted ordering of the Ia and IIa states in the **3R$_D$** and **5R$_D$** dimers is provided by comparing the monomer and dimer fluorescence line shapes. The fluorescence spectra of **5R** and **5R$_D$** both have distinct vibronic structure, which suggests that the emitting state has the same nature, namely the 1Bu state of the monomer. In contrast, the fluorescence profile of **3R$_D$** is featureless and does not show the vibrational bands of **3R**. It closely resembles the emission of paracyclophane[19] and suggests that the **3R$_D$** emission originates from the phane state.

Conclusion

Figure 4b shows that the lowest energy absorption band in **3R** (II) leads to electron delocalization over a large portion of the molecule. Also, the strongest coherences are localized over the olefins. For **5R** the outer rings participate less in (II). With increasing excitation frequency the electronic modes become more localized on the repeat units. In other words, they become more localized on the individual aromatic rings.

It follows from our calculations that the Ia state (which may be traced to the **Pc** core) in **3R$_D$** is nearly isoenergetic to state IIa, which is more delocalized. An important difference between Ia and IIa is in the distribution of electronic coherences across the electronic mode. Ia and IIa have the strongest coherences in the off-diagonal and diagonal directions, respectively. This

further leads to the vanishing oscillator strength of Ia and the strong transition dipole of IIa. Therefore, while the distribution of electron density appears similar in these two states, Ia is forbidden and IIa is fully allowed. For **5R$_D$** the IIa state is substantially lower in energy than the corresponding Ia state. It is more likely that the emitting state is directly related to this state. Otherwise the overall electronic description is similar.

The splitting of spectra in molecular aggregates is usually interpreted using the Frenkel Exciton model, which assumes that the electron density is localized within each unit. The resulting Davydov splitting originates from purely electrostatic (e.g. dipole−dipole and higher multipole) interactions among chromophores.[38] The IIa−IIb splitting observed in the spectra is reminiscent of Davydov splittings. However, our CEO analysis shows that the interaction between monomers is not electrostatic, but involves electron exchange. This is clearly seen by the off-diagonal blocks between monomers in Figure 5, which represent a charge separation of an electron and a hole between the monomers. These off-diagonal coherences should vanish identically for the Davydov Model. The strong coupling through the paracyclophane core provides a conduit for electron delocalization. Differences in the optical properties of the "arms" and the "dimers" are a consequence of strong electronic coherence between the two fragments brought about by their close proximity. The Davydov model cannot be used for computing these splittings.

Finally, these results highlight the effect of contact location on the strength of delocalization between fragments. In the "terminal" contact pairs,[19] the optical properties could be neatly explained in terms of excitations that migrated to the phane state (short arms) or that remained localized in the chromophores (longer arms). Choosing a trajectory such that the inner rings are brought into close proximity prevents an analogous dissection of parts. The optical properties and electronic description of the criss-cross delocalized pairs indicate that the excitation is delocalized across the entire molecule. In a sense there is strong mixing of the phane and the "antenna" or "chromophore" states.

Experimental Section

General Details. ^{1}H and ^{13}C NMR spectra were recorded on a Varian Unity 400 NMR spectrometer. UV−vis absorption spectra were measured on a Shimadzu UV-2401 PC diode array spectrophotometer and photoluminescence spectra on a Spex Fluoromax-2 spectrometer. High-resolution mass spectrometry was performed on a VG-70SE Double Focusing System with FAB ionization sources. Purification of final products was done with Chromatotron form Harrison Research Company. Chromatotron rotor was coated with Merk TLC grade 7749 silica gel. Reagents were obtained from Aldrich and used as received. The fluorescence quantum yield standard 9,10-diphenylanthracene was obtained from Aldrich and was purified by column chromatography on silica using petroleum ether as eluent.

(38) (a) Kasha, M.; Rawls, H. R.; El-Bayoumi, M. A. *Pure Appl. Chem.* **1965**, *11*, 371. (b) Silinish, E. A.; Capek, V. *Organic Molecular Crystals*; American Institute of Physics: New York, 1994. (c) Pope, M.; Swenberg, C. E. *Electronic Processes in Organic Crystals*; Clarendon Press: New York, 1982.
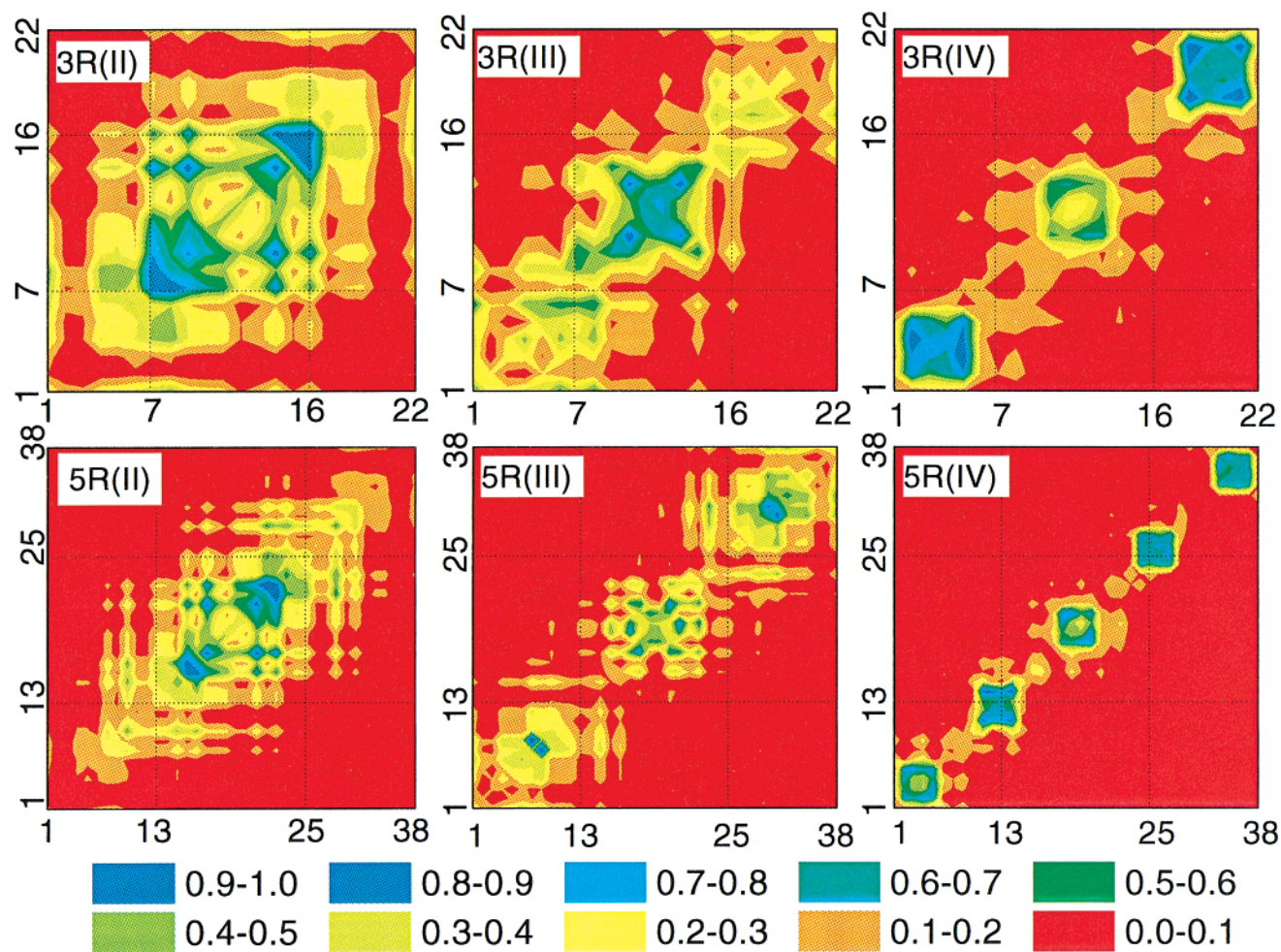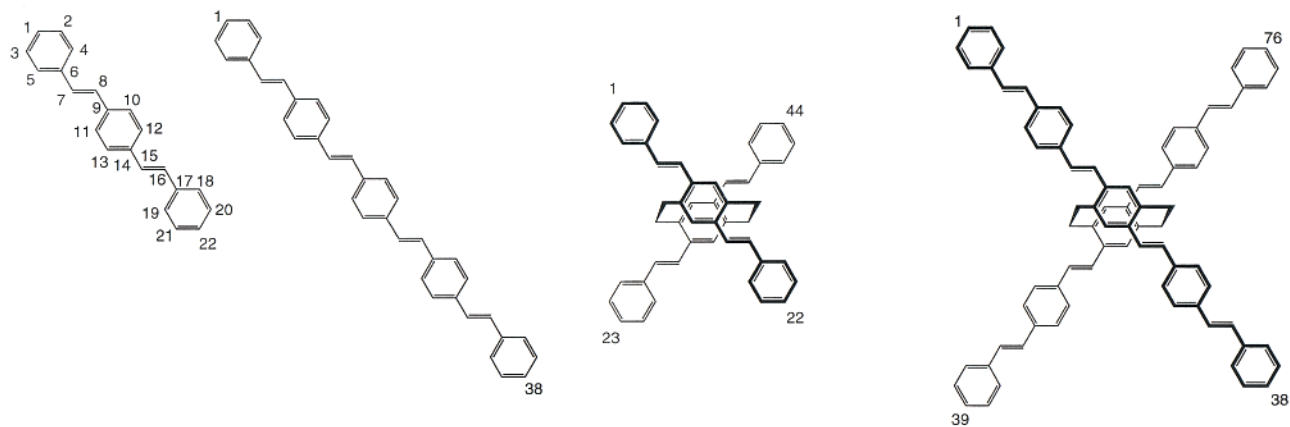
Figure 4. (a, top) Labeling scheme for the carbon atoms in **3R**, **3R_D**, **5R**, and **5R_D**. (b, bottom) Contour plots of electronic modes which dominate the optical absorption of monomers **3R** and **5R**. The axis labels represent the individual carbon atoms as labeled in part a. The panels indicate the molecule and the electronic mode (Figure 3) (e.g. 3R(II) is mode II of **3R**). The color code is given in the bottom row.

Solutions for fluorescence measurements were adjusted to a specific concentration so that the maximum absorbance was ≤0.1. Solutions were degassed with argon in a 1 cm standard quartz cell before fluorescence measurements. The quantum yield was calculated from the relation:[39]

$$\Phi_u = \Phi_s[(A(\lambda)_s F_u n_u^2)/(A(\lambda)_u F_s n_s^2)]$$

where the subscripts s and u indicate the standard and unknown sample,

$A(\lambda)$ corresponds to the absorbance of the solution at the exciting wavelength λ, F is the integrated luminescence spectrum, and n is the index of refraction for the solvent carrying the unknown and the standard at the sodium D line. The standard fluorophore for solution measurements[40] was 9,10-diphenylanthracene[40] with $\Phi_s = 0.90$.

2,5-Dimethyl-1,4-bis(4-*tert*-butylstyryl)benzene (3R). A round-bottom flask was charged with a Teflon-coated stir bar, 2,5-dibromo-*p*-xylene (792 mg, 3 mmol), 4-*tert*-butylstyrene (4.8 g, 30 mmol), Pd(OAc)₂ (33.7 mg, 0.15 mmol), K₂CO₃ (4.14 g, 30 mmol), Nbu₄Br

(39) Eaton, D. F. *Pure Appl. Chem.* **1988**, *60* (7), 1107.

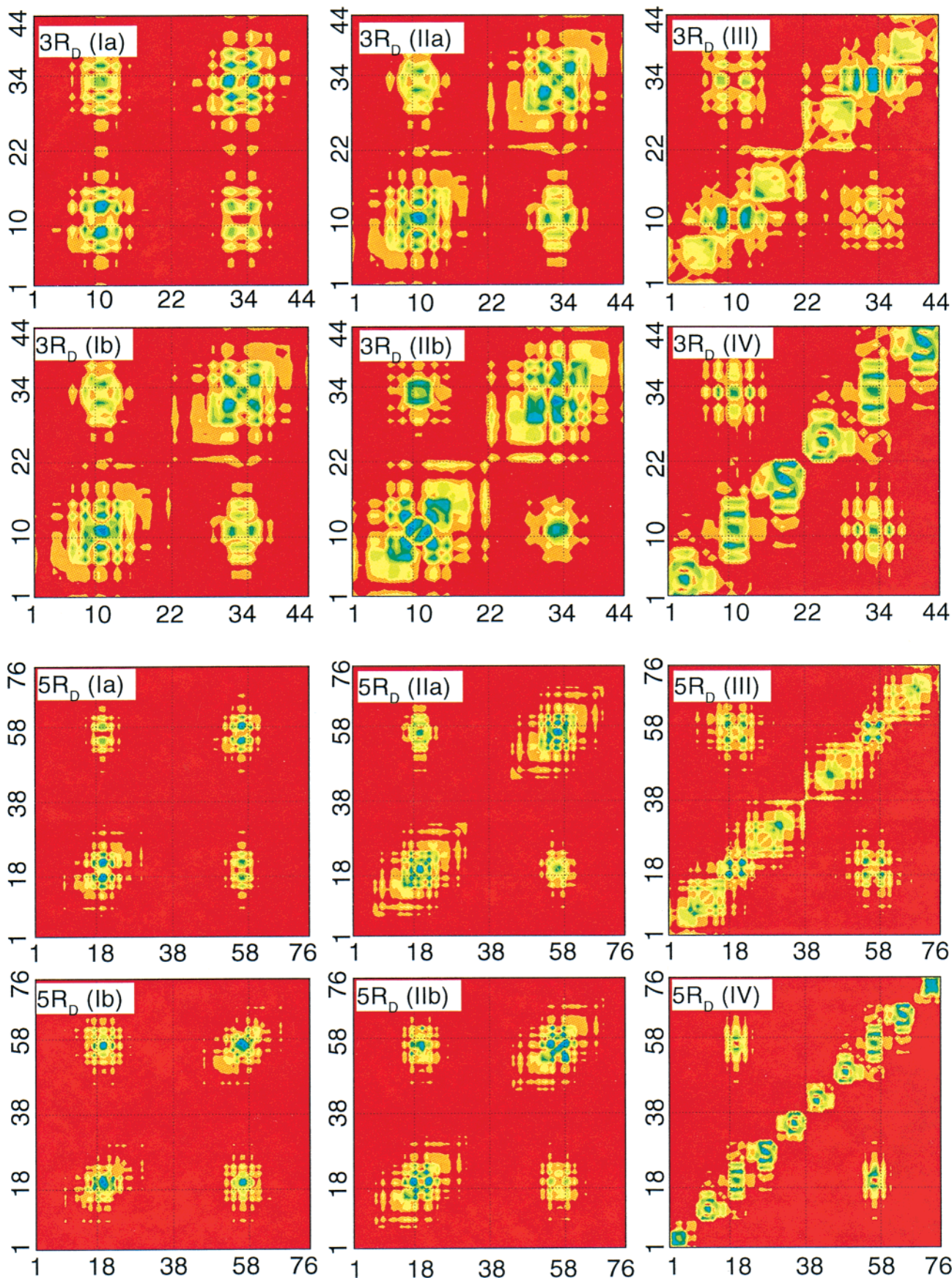(40) Hamai, S.; Hirayama, F. *J. Phys. Chem.* **1983**. *87*, 83.

Figure 5. Contour plots of electronic modes that dominate the optical absorption of dimers **3R$_D$** and **5R$_D$**. The axis labels represent the individual carbon atoms as labeled in Figure 4a. The panels indicate the molecule and the electronic mode (Figure 3). The color code is given in Figure 4b.

(3.87 g, 12 mmol), and DMA (27 mL). The reaction mixture was purged with nitrogen and heated at 100 °C for 3 days. The reaction was cooled to room temperature, diluted with CH$_2$Cl$_2$, and washed with brine. The organic layer was dried with Na$_2$SO$_4$ and concentrated. The residual

liquid (containing a small amount of DMA) was precipitated with hexanes and collected by filtration. The crude product was purified with a Chromatotron on a 2 mm silica-coated rotor (1:9 CHCl$_3$/hexanes) to yield 0.7 g (55%) of a white solid. ^{13}C NMR (100 MHz, CDCl$_3$) δ 150.9, 135.7, 135.2, 133.6, 129.4, 127.2, 126.5, 125.8, 125.6, 34.8, 31.5, 19.8 ppm. ^{1}H NMR (400 MHz, CDCl$_3$) δ 7.41 (d, J = 8.3 Hz, 4H), 7.43 (s, 2H), 7.40 (d, J = 8.3 Hz, 4H), 7.28 (d, J = 16.1 Hz, 2H), 7.00 (d, J = 16.1 Hz, 2H), 2.43 (s, 6H), 1.35 (s, 18H) ppm. Exact mass (FAB, NBA) for M$^+$ (C$_{32}$H$_{38}$): calculated 422.2974; found 422.2958.

2,5-Dimethyl-1,4-bis[4-(4′-*tert*-butylstyryl)styryl]benzene (5R). A round-bottom flask was charged with a Teflon-coated stir bar, 2,5-dibromo-*p*-xylene (153 mg, 0.58 mmol), 4-*trans*-4,4′-*tert*-butylvinyl-stilbene (915 mg, 3.5 mmol), Pd(OAc)$_2$ (6.5 mg, 0.03 mmol), K$_2$CO$_3$ (800 mg, 5.8 mmol), NBu$_4$Br (748 mg, 2.3 mmol), and DMA (8 mL). The reaction mixture was purged with nitrogen and heated at 100 °C for 3 days. The reaction was cooled to room temperature, diluted with CH$_2$Cl$_2$, and washed with brine. The organic layer was dried with Na$_2$SO$_4$ and concentrated. The residual liquid (containing a small amount of DMA) was precipitated with hexanes and collected by filtration. The crude product was purified with a Chromatotron on a 2 mm silica-coated rotor (1:5 CHCl$_3$/hexanes) to yield 91 mg (25%) of yellow solid. ^{1}H NMR (400 MHz, CDCl$_3$) δ 7.52 (s, 8H), 7.47 (d, J = 8.5 Hz, 4H), 7.46 (s, 2H), 7.39 (d, J = 8.5 Hz, 4H), 7.33 (d, J = 16.1 Hz, 2H), 7.10 (dd, J = 16.6 Hz, 4H), 7.04 (d, J = 16.1 Hz, 2H), 2.43 (s, 6H), 1.35 (s, 18H) ppm. The compound was too insoluble to obtain an accurate ^{13}C NMR spectrum. Exact mass (FAB, NBA) for M$^+$ (C$_{48}$H$_{50}$): calculated 626.3912; found 626.3901.

4,7,12,15-Tetra(4-*tert*-butylstyryl)[2.2]paracyclophane (3R$_D$). A round-bottom flask was charged with a Teflon-coated stir bar, 4,7,-12,15-tetrabromoparacyclophane (200 mg, 0.39 mmol), 4-*tert*-butyl-styrene (1.84 g, 11.5 mmol), Pd(OAc)$_2$ (12 mg, 0.054 mmol), K$_2$CO$_3$ (539 mg, 3.9 mmol), NBu$_4$Br (502 mg, 1.56 mmol), and DMA (14 mL). The reaction mixture was purged with nitrogen and heated at 100 °C for 4 days. The reaction was cooled to room temperature, diluted

with CH$_2$Cl$_2$, and washed with brine. The organic layer was dried with Na$_2$SO$_4$ and concentrated. The residual liquid (containing a small amount of DMA) was precipitated with methanol and collected by filtration. The crude product was purified with Chromatotron on 2 mm silica-coated rotor (1:9 CHCl$_3$/hexanes) to yield 146 mg (44%) of yellow solid. ^{1}H NMR (400 MHz, CDCl$_3$) δ 7.45 (dd, J = 8.6 Hz, 16H), 7.20 (d, J = 16.1 Hz, 4H), 6.94 (d, J = 16.1 Hz, 4H), 3.57 (m, 4H), 2.87 (m, 4H), 1.40 (s, 36H) ppm. ^{13}C NMR (100 MHz, CDCl$_3$) δ 150.6, 137.7, 136.6, 134.9, 128.2, 127.9, 126.3, 125.6, 124.7, 34.6, 33.0, 31.3 ppm. Exact mass (FAB, NBA) for M$^+$ (C$_{64}$H$_{72}$): calculated 840.5649; found 840.5634.

4,7,12,15-Tetra[4-(4′-*tert*-butylstyryl)styryl][2.2]paracyclo-phane (5R$_D$). A round-bottom flask was charged with a Teflon-coated stir bar, 4,7,12,15-tetrabromoparacyclophane (200 mg, 0.39 mmol), *trans*-4,4′-*tert*-butylvinylstilbene (1.39, g, 5.3 mmol), Pd(OAc)$_2$ (20 mg, 0.09 mmol), K$_2$CO$_3$ (539 mg, 3.9 mmol), NBu$_4$Br (502 g, 1.56 mmol), and DMA (25 mL). The reaction mixture was purged with nitrogen and heated at 100 °C for 4 days. The reaction was cooled to room temperature, diluted with CH$_2$Cl$_2$, and washed with brine. The organic layer was dried with Na$_2$SO$_4$ and concentrated. The residual liquid was precipitated with methanol and collected by filtration. The crude product was purified with a Chromatotron on 2 mm silica-coated rotor (3:7 CHCl$_3$/hexanes) to yield 88 mg (18%) of a yellow solid. ^{1}H NMR (400 MHz, CDCl$_3$) δ 7.56 (d, J = 8.5 Hz, 8H), 7.50 (dd, J = 8.5 Hz, 16H), 7.42 (d, J = 8.5 Hz, 8H), 7.23 (d, J = 16.0 Hz, 4H), 7.16 (dd, J = 16.3 Hz, 8H), 7.03 (s, 4H), 6.95 (d, J = 16.0 Hz, 4H), 3.62 (m, 4H), 2.92 (m, 4H), 1.40 (s, 36H) ppm. The compound was too insoluble to obtain an accurate ^{13}C NMR spectrum. Exact mass (FAB, NBA) for M$^+$ (C$_{96}$H$_{96}$): calculated 1248.7512; found 1248.7499.

JA991611Y